Advanced modeling of shrinkage porosity in castings

IOP Conf. Series: Materials Science and Engineering **861** (2020) 012022 doi:10.1088/1757-899X/861/1/012022

Advanced modeling of shrinkage porosity in castings

P Esser[1], C Schankies[1], V Khalajzadeh[2] and C Beckermann[2]

[1] MAGMA Gießereitechnologie GmbH, Kackertstr. 11, 52072 Aachen, Germany
[2] Dept. of Mechanical Engineering, University of Iowa, Iowa City, IA 52242, USA

E-mail: p.esser@magmasoft.de, becker@engineering.uiowa.edu

Abstract. Porosity due to solidification shrinkage is a troublesome defect in all types of metal castings. It limits the performance of cast components by adversely affecting the material's strength, fatigue and creep properties. By reliably predicting porosity in casting process simulation, it can be minimized or eliminated. Here, a newly developed model for predicting porosity is presented. The model is based on the recent discovery that all shrinkage porosity nucleates and grows in regions of a casting where the solid fraction is the lowest. It calculates the feeding flows and pressure distribution in the liquid while accounting for the liquid density variation during cooling and solidification. It predicts the location, extent and amount of all types of shrinkage porosity in a casting, including riser pipes and large internal holes, surface sinks, and distributed micro-shrinkage. The model is numerically implemented in a standard casting simulation code. Comparisons to measurements in specially made steel castings demonstrate the capability of the model to accurately predict various types of shrinkage porosity.

1. Introduction

In metal casting, shrinkage porosity is a widespread problem. It forms during solidification, when liquid melt can no longer feed the loss of volume during contraction. This leads to defects (porosities) in the casting, which affect the quality and mechanical properties. In general, there are three types of porosity in a casting: surface sinks, internal macro-porosity and (internal) micro-porosity (see figure 1). We will present a mathematical model that can predict these types of defects adequately:

- It accurately predicts location, amount and appearance of porosity.
- It predicts locations of porosity nucleation and growth.
- It predicts the stages of surface and internal porosity formation.

This model is integrated into commercial simulation software.

2. Computational model

In order to model the formation of porosities, we use the following physical concepts:

- Porosity nucleates where solid fraction is the lowest.
- Feeding flows are calculated.
- Surface and internal porosity are calculated.

A schematic diagram of a solidifying casting volume is shown in figure 2. Multiple regions of porosity can form simultaneously. The boundary conditions at the casting surface and on the porosity containing regions are indicated in figure 2(a) and figure 2(c), respectively. The model allows for a representative elementary volume to be composed of three phases: solid (s), liquid (ℓ) and porosity (p).

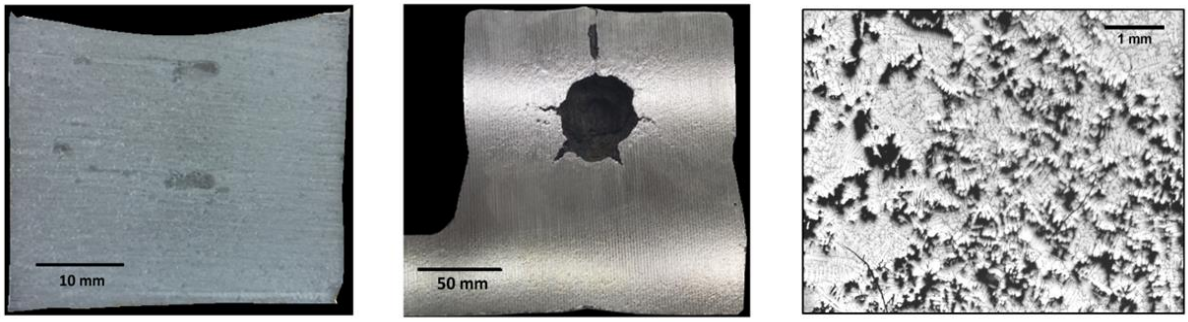

Figure 1. Various types of shrinkage porosity in castings: (a) a sink on the top surface of a cast aluminum block, (b) internal macro-shrinkage hole in a steel casting, and (c) distributed internal micro-shrinkage porosity.

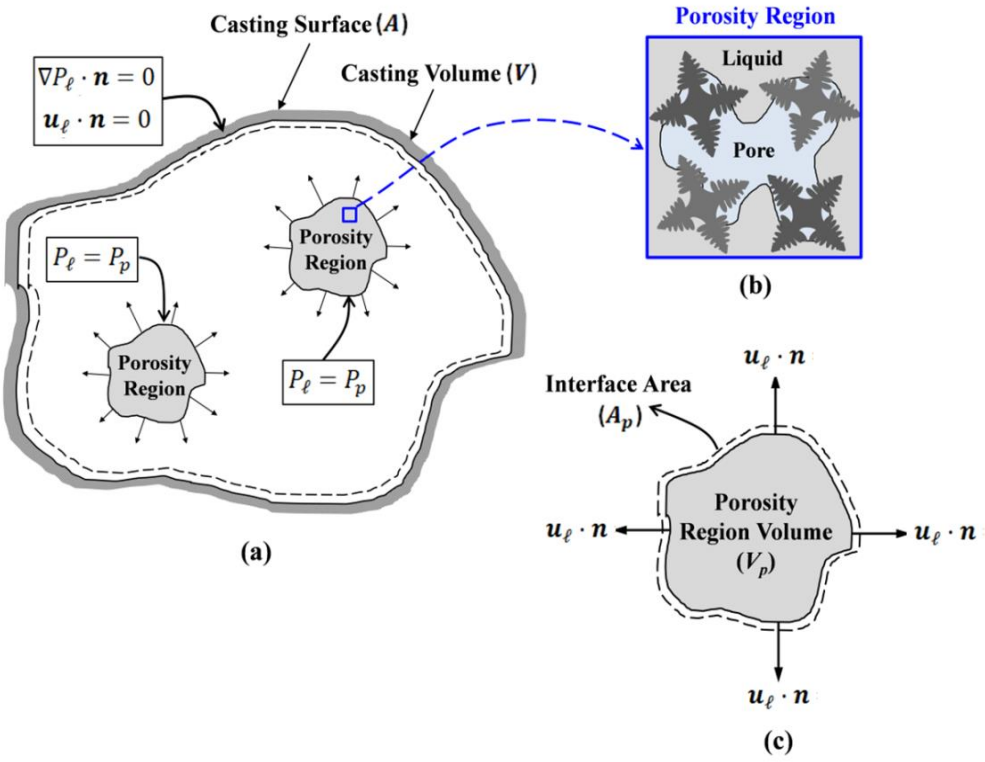

Figure 2. Schematic diagram of a solidifying casting with porosity: (a) casting volume with multiple porosity containing regions, (b) representative elementary volume containing solid, liquid and porosity, and (c) single porosity containing region

Using "g" to denote the volume fraction of a given phase, and the phases indicated by subscripts, the volume fractions must satisfy $g_\ell + g_s + g_p = 1$, as shown schematically in figure 2(b).

Key assumptions in the model are:

- Solid and porosity phases are stationary; they cannot move during solidification; however, solid may be replaced by porosity if the solid fraction is below a certain coherency limit.
- Flow of the liquid melt is driven by mixture density changes only; buoyancy-driven flow during solidification is neglected.

- Density is temperature-dependent above the solidus temperature and assumed constant when the metal is solid; the density of the gases inside of shrinkage pores is neglected.

The governing equations for the feeding flow and the procedures used for predicting the evolution of the pore volume fraction are given in the following sub-sections. The model assumes that the results from a standard thermal simulation of the casting are available. This includes the evolution of the temperature and solid fraction fields throughout the solidification process. The heat transfer is assumed to be unaffected by the porosity.

2.1. Continuity and momentum equations

Mass is conserved according to a mixture continuity equation

$$\frac{\partial \bar{\rho}}{\partial t} + \nabla \cdot (\rho_\ell \, \boldsymbol{u}_\ell) = 0 \tag{1}$$

where t is time, ρ_ℓ is the liquid density, and $\boldsymbol{u}_\ell$ is the superficial liquid velocity vector. The three-phase mixture density $\bar{\rho}$ is defined as $\bar{\rho} = \rho_s g_s + \rho_\ell g_\ell + \rho_p g_p$. The feeding flow in the mushy zone is assumed to be a creeping flow in a porous medium of variable permeability. For such flows the momentum equation is given by Darcy's law,

$$\nabla P_{\ell,t} = -\frac{\mu_\ell \boldsymbol{u}_\ell}{K} + \rho_\ell \, \boldsymbol{g} \tag{2}$$

where $P_{\ell,t}$ is the total liquid pressure, μ_ℓ is the dynamic viscosity of the melt, K is the permeability of the mush, and $\boldsymbol{g}$ is the gravity vector. Equation (2) is also used in the pure liquid regions, by setting the permeability to a sufficiently large value, $K_{\max}$. The total liquid pressure ($P_{\ell,}$) is the sum of the dynamic liquid pressure (P_ℓ) and the hydrostatic pressure (P_h), i.e., $P_{\ell,} = P_\ell + P_h$. Applying the gradient operator to this equation gives $\nabla P_{\ell,} = \nabla P_\ell + \nabla P_h$, where the hydrostatic pressure is given by $\nabla P_h = \rho_\ell \, \boldsymbol{g}$. Combining this and equation (2), the gravity term cancels and equation (2) simplifies to

$$\nabla P_\ell = -\frac{\mu_\ell \boldsymbol{u}_\ell}{K} \tag{3}$$

The permeability of the mush is a function of solid fraction (g_s) according to the Kozeny–Carman equation

$$K = K_0 \frac{(1 - g_s)^3}{g_s^2} \tag{4}$$

where K_0 is an adjustable constant permeability coefficient. To avoid division by zero in equation (3), a suitable minimum allowable value for the permeability, $K_{\min}$, is introduced. To ensure well-posedness of equation (4), suitable boundary conditions are needed. Here it is assumed that P_ℓ within regions having porosity is equal to the pore pressure: $P_\ell|_{\text{Porosity}} = P_{p,}$ implying that surface tension effects are neglected. The value of the pore pressure P_p depends on the location in the casting. At an atmosphere-metal interface the pore pressure is assumed to be atmospheric: $P_p = P_{\text{atm}}$, at a mold-metal interface it is equal to some pre-defined mold atmosphere pressure: $P_p = P_{\text{mold}}$ and for internal porosity, the pores are assumed to be vacuum (negligible density), $P_p = 0$. By forcing the dynamic pressure to a uniform value, the liquid velocities vanish inside of porosity forming regions. Assuming for simplicity that ρ_ℓ in equations (1) and (2) is constant, equations (1) and (3) can be combined to form an equation for determining the pressure P_ℓ throughout the casting during solidification

$$\nabla \cdot \left(\frac{K}{\mu_\ell} \nabla P_\ell\right) = \frac{1}{\rho_\ell} \frac{\partial \bar{\rho}}{\partial t} \tag{5}$$

As shown in figure 3, the boundary condition for the above equation is given by a zero-mass flux condition at the casting surface, which can be written as $(\boldsymbol{u}_\ell \cdot \boldsymbol{n})_{\text{surface}} = (\nabla P_\ell \cdot \boldsymbol{n})_{\text{surface}}$, where $\boldsymbol{n}$ is the normal vector on the surface. Using this boundary condition and forcing the pressure in the porosity containing regions to $P_\ell|_{\text{Porosity}} = P_p$, the pressure distribution P_ℓ in the casting can be determined by solving equation (5).

2.2. Pore nucleation model

The presented pore nucleation model is based on the one developed by Khalajzadeh *et al.* [1]. Surface sinks and internal porosity do not evolve at the same time. Surface sinks develop first and internal porosity forms in a second stage. The transition between the two stages is modeled by introducing the critical solid fraction $g_{s,\text{sur}}$. When the solid fraction at the surface is below this critical value, a surface sink can form. Once the solid fraction everywhere on the surface is above $g_{s,\text{sur}}$ the surface becomes rigid and internal porosity can nucleate. The pore nucleation model is based on the inequality form of the Young-Laplace equation, which is given in the present study by

$$P_p - P_{\ell,t} \geq P_\sigma \tag{6}$$

where $P_{\boldsymbol{\sigma}}$ is a capillary pressure due to surface tension. As found by Khalajzadeh *et al.* [1], the capillary pressure $P_{\boldsymbol{\sigma}}$ in equation (6) can be taken as a linear function of the solid fraction as

$$P_\sigma = P_{\sigma,0}\, g_s, \tag{7}$$

where $P_{\boldsymbol{\sigma},0}$ is a reference capillary pressure at a solid fraction of unity. As in Khalajzadeh *et al.* [1], the Young-Laplace inequality is implemented in the model through a so-called Π parameter, which is defined as

$$\Pi = P_{\ell,t} - (P_p - P_\sigma) \tag{8}$$

Porosity is thus nucleated where the Π parameter is the lowest. To make the nucleation calculations numerically robust, porosity is nucleated where the Π value falls within a small dimensionless interval ε_{nuc} according to:

$$\left|\frac{\Pi - \Pi_{\min}}{\Pi_{\max} - \Pi_{\min}}\right| < \varepsilon_{\text{nuc}} \tag{9}$$

where $\Pi_{\min}$ is the instantaneous minimum Π value in the computational domain and $\Pi_{\max}$ is the maximum possible Π value. Physically, the adjustable parameter ε_{nuc} controls the initial size of a newly nucleated porosity region. Other details of the pore nucleation model can be found in [1].

2.3. Pore growth model

As shown in figure 3(a), multiple regions of porosity can nucleate and grow in a casting simultaneously. Each region is a grouping of connected computational cells having $g_p > 0$. The volume and surface area of each porosity forming region are denoted by V_p and A_p, respectively, as shown in figure 3(c). The average pore growth rate $(d\bar{g}_p/dt)$ for each porosity containing region is calculated by integrating the mass conservation equation, equation (1), over V_p. Using the divergence theorem for the second term in equation (1) yields

$$\int_{V_p} \left(\frac{\partial \bar{\rho}}{\partial t}\right) dV + \int_{A_p} (\rho_\ell \boldsymbol{u}_\ell) \cdot \boldsymbol{n}\, dA = 0 \tag{10}$$

The density $\bar{\rho}$ should be distinguished from the solid-liquid mixture density in the absence of porosity, which is given by, $\bar{\rho}^{SL} = \rho_s, g_s^{SL} + \rho_\ell g_\ell^{SL}$, where $g_s^{SL} + g_\ell^{SL} = 1$. The density $\bar{\rho}^{SL}$ is assumed to be known as a function of temperature for a given metal alloy. Assuming that $g_s^{SL} = g_s$ and $\rho_p \ll \rho_s, \rho_\ell$ yields the following equation for the three-phase density

$$\bar{\rho} = \bar{\rho}^{SL} - \rho_\ell g_p \tag{11}$$

Assuming that ρ_ℓ in equation (11) is constant and that the pore growth rate is uniform within each V_p, substitution of equation (11) into equation (10) results in

$$\frac{d\bar{g}_p}{dt} = \frac{1}{\rho_\ell |V_p|} \int_{V_p} \left(\frac{\partial \bar{\rho}^{SL}}{\partial t} \right) dV + \frac{1}{|V_p|} \int_{A_p} \boldsymbol{u}_\ell \cdot \boldsymbol{n} \, dA \tag{12}$$

Equation (12) allows for the calculation of the average pore growth rate in each porosity forming region from the knowledge of the average solid-liquid mixture density variation within V_p and the feeding flow velocities normal to the boundary A_p. The average porosity increase from equation (12) is then evenly distributed over all active computational cells within each V_p to determine the local time rate of change in the pore fraction according to [1].

The pore volume fraction is typically allowed to increase until a computational cell becomes empty of liquid, i.e., when $g_s + g_p = 1$. This condition, however, would often result in the local pore fraction never being able to approach unity. A pore fraction of unity occurs, for example, when a surface sink or internal hole is free of solid. For the pore volume fraction to reach unity, the previously grown solid at that location must have moved or been pushed away by the growing porosity, which is frequently referred to as mass feeding. As in Khalajzadeh *et al.* [1], mass feeding is modeled by introducing an adjustable parameter called the coherency solid fraction $g_{s,\text{coh}}$. The maximum pore volume fraction, $g_{p,\max}$, is then given by

$$g_{p,\,\max} = \begin{cases} 1, & g_s < g_{s,\,\text{coh}} \\ 1 - g_s, & g_s \geq g_{s,\,\text{coh}} \end{cases} \tag{13}$$

The two critical solid fractions $g_{s,\text{sur}}$ and $g_{s,\text{coh}}$ take typically the same value [1]. When a computation cell reaches the maximum pore fraction, it is designated as inactive. Once a pore forming region has no more active cells, but solidification is not yet complete, porosity can spread beyond the originally nucleated volume. As in Khalajzadeh *et al.* [1], such spreading of pore forming regions is modeled using the same Π parameter introduced in the previous subsection. Computational cells that neighbor a cell with porosity already present are activated when their Π parameter falls within the interval

$$\left| \frac{\Pi - \Pi_{\min}}{\Pi_{\max} - \Pi_{\min}} \right| < \varepsilon_{\text{layer}} \tag{14}$$

The small dimensionless number $\varepsilon_{\text{layer}}$ is an adjustable model parameter that controls the rate of spreading of porosity regions. It is emphasized here that the use of the Π parameter in both the pore nucleation and growth models was developed by some of the authors through careful comparisons with real-time video radiography experiments [1].

3. Experiments and simulation

To validate the model, castings were made from high manganese (Mn) steel in chemically bonded olivine sand [2]. The geometry is shown in figure 3. It consists of a gating system, a riser, two steps of different thickness, a thinner plate section, and a thick end block. The thermal simulation was calibrated with the help of thermocouples [3].

The experimentally observed porosity is shown in figure 4, while the porosity predicted by the present model, using the parameters listed in table 1, is shown in figure 5. We see in general good agreement of the model predictions with the porosity observed in the casting.

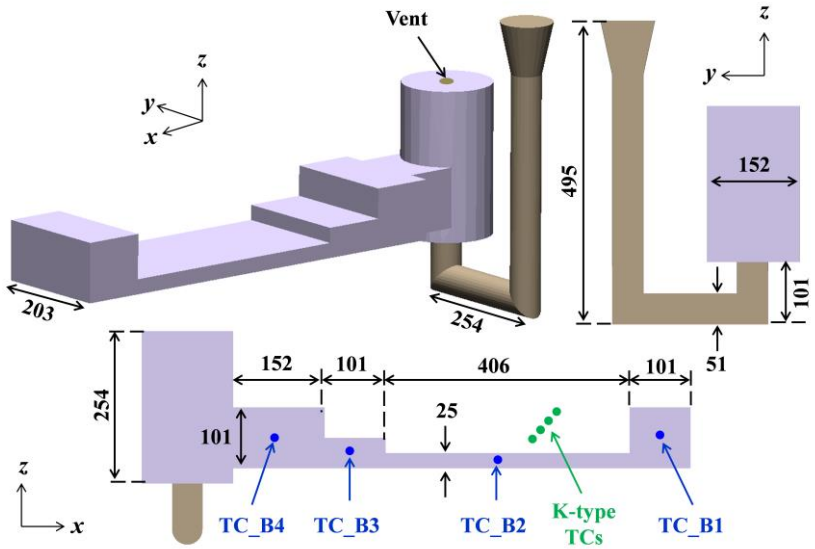

Figure 3. Mn-steel casting geometry used in the experiments; the dimensions are in millimeter (mm).

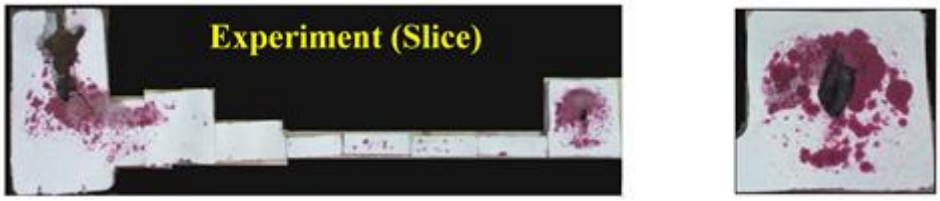

Figure 4. Porosity distribution observed in the Mn-steel casting: vertical slices through the casting at mid-width, with the red areas showing microporosity that is visualized using dye penetration testing.

Figure 5. Porosity predictions obtained by the present model for the Mn-steel casting shown in figure 4.

Table 1. Material properties and model parameter used in the simulation

Parameter	Value
K_0 (m^3)	1.7e-9
$K_{\min}$ (m^3)	1.0e-16
$K_{\max}$ (m^3)	1.0e-6
$g_{s,\text{sur}}$ (-)	0.625
$g_{s,\text{coh}}$ (-)	0.625
$\varepsilon_{\text{layer}}$ (-)	5.0e-2
ε_{nuc} (-)	5.0e-3
P_{atm} (bar)	1.101325
$P_{\boldsymbol{\sigma},0}$ (bar)	P_{atm}
P_{mold} (bar)	0.4 P_{atm}
ρ_s (kg/m^3)	7124
ρ_ℓ (kg/m^3)	6894
μ_ℓ (Pa.s)	8.57e-3

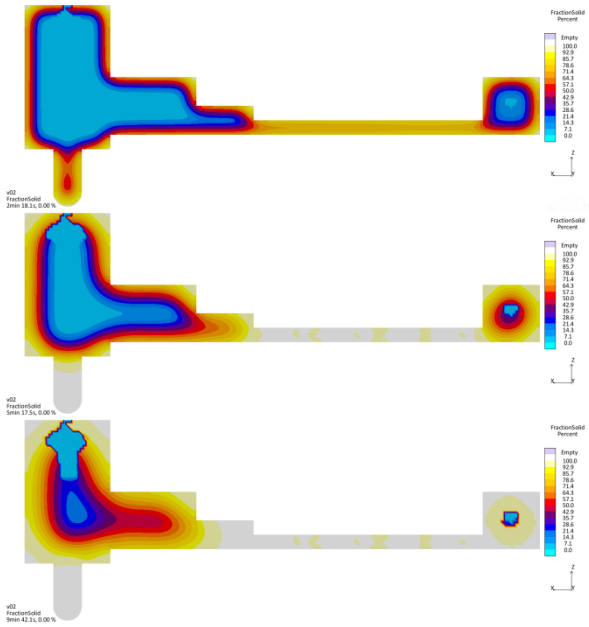

Figure 6. Fraction solid (50%, 75%, 90% solidified).

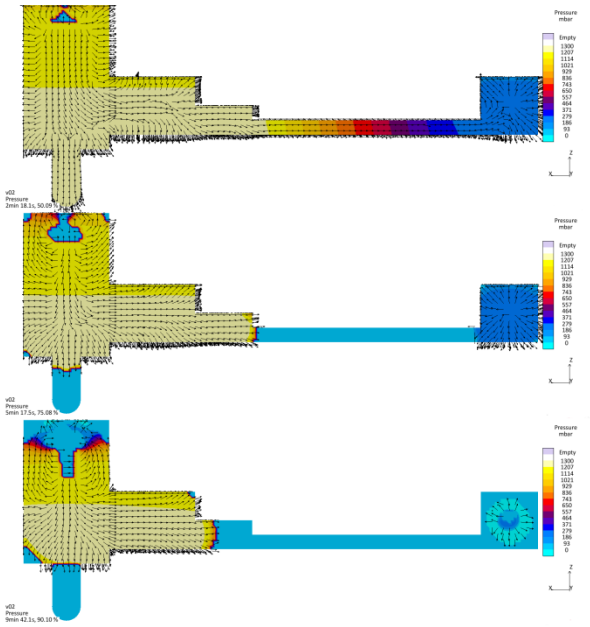

Figure 7. Total pressure and feeding velocity vectors (50%, 75%, 90% solidified).

Other results of the simulation are shown in figure 6 and figure 7. These show the evolution of the fraction solid g_s from the thermal simulation (figure 6) and the total pressure P_ℓ and feeding velocity vectors $\boldsymbol{u}_\ell$ from the present model (figure 7). The results are shown at the states of 50%, 75%, 90% solidified cells in all casting materials. Until almost 50%, all shrinkage of the metal during cooling and solidification is fed by the gating system. The total pressure distribution is mostly hydrostatic, because the dynamic pressure variations are still very small. The top of the riser is connected to the atmosphere through a small vent that induces a shrinkage pipe at that location once the pressure falls below atmospheric pressure. At 50% solidified cells, the permeability in the thin plate section is low enough that the liquid flow feeding the end block from the riser creates a large pressure drop. Eventually, the pressure in the end block approaches vacuum and porosity nucleates in the thermal center of the end block where the solid fraction is lowest. At 75%, the thin plate section between the riser and the end

block is fully solidified and the pressure inside the block is forced by the internal porosity in the center of the block. Small areas of microporosity can be observed in the thin plate section. The rest of the casting continues to be fed by the downward growing hole at the top of the riser. At 90%, the riser pipe acquires a more conical shape and extends over the top one-third of the riser. Eventually, microporosity forms next to and below the open riser pipe and in the larger step (figure 5).

4. Conclusions

A model for the prediction of shrinkage porosity in metal castings is developed. It is based on the solution of the basic equations for the feeding flow and pressure distribution during solidification and an extended version of the pore nucleation and growth model of Khalajzadeh *et al.* [1]. The model uses the temperature and solid fraction results from a thermal simulation and predicts all kinds of shrinkage porosity, including surface sinks and riser pipes, open shrinkage holes internal to the casting, and micro porosity dispersed between dendrite arms. Good agreement is obtained with observations made in an experimental Mn-steel sand casting. The shape of the riser pipe, the open shrinkage hole in the thermal center of the end block, and the microporosity in the thin plate section and around the larger holes are all predicted correctly. No surface sinks were observed or predicted to form. Results from another test casting with surface sinks, including quantitative comparisons between measured and predicted pore fraction values, can be found in Khalajzadeh *et al.* [1,2].

References

[1] Khalajzadeh V, Goettsch D and Beckermann C 2019 *Metall. Mater. Trans. A* **50** 757-71
[2] Khalajzadeh V 2018 *Modeling of shrinkage porosity defect formation during alloy solidification* PhD thesis (University of Iowa, Iowa City, IA)
[3] MAGMASOFT® MAGMA GmbH Aachen Germany